Optics Letters

Experimental implementation of generalized transitionless quantum driving

Chang-Kang Hu,[1,2,†] Jin-Ming Cui,[1,2,†] Alan C. Santos,[3,4] Yun-Feng Huang,[1,2,*] Marcelo S. Sarandy,[3,5] Chuan-Feng Li,[1,2,6] and Guang-Can Guo[1,2]

[1]CAS Key Laboratory of Quantum Information, University of Science and Technology of China, Hefei 230026, China
[2]Synergetic Innovation Center of Quantum Information and Quantum Physics, University of Science and Technology of China, Hefei 230026, China
[3]Instituto de Física, Universidade Federal Fluminense, Av. Gal. Milton Tavares de Souza s/n, Gragoatá, 24210-346 Niterói, Rio de Janeiro, Brazil
[4]e-mail: ac_santos@id.uff.br
[5]e-mail: msarandy@id.uff.br
[6]e-mail: cfli@ustc.edu.cn
*Corresponding author: hyf@ustc.edu.cn

Received 7 May 2018; revised 29 May 2018; accepted 29 May 2018; posted 30 May 2018 (Doc. ID 330948); published 27 June 2018

It is known that high intensity fields are usually required to implement shortcuts to adiabaticity via transitionless quantum driving (TQD). Here, we show that this requirement can be relaxed by exploiting the gauge freedom of generalized TQD, which is expressed in terms of an arbitrary phase when mimicking the adiabatic evolution. We experimentally investigate the performance of generalized TQD in comparison to both traditional TQD and adiabatic dynamics. By using a $^{171}Yb^{+}$ trapped ion hyperfine qubit, we implement a Landau–Zener adiabatic Hamiltonian and its (traditional and generalized) TQD counterparts. We show that the generalized theory provides energy-optimal Hamiltonians for TQD, with no additional fields required. In addition, the optimal TQD Hamiltonian for the Landau–Zener model is investigated under dephasing. Even using less intense fields, optimal TQD exhibits fidelities that are more robust against a decohering environment, with performance superior to that provided by the adiabatic dynamics. © 2018 Optical Society of America

OCIS codes: (270.0270) Quantum optics; (270.5585) Quantum information and processing; (020.0020) Atomic and molecular physics.

https://doi.org/10.1364/OL.43.003136

Transitionless quantum driving (TQD) [1–3] is a useful technique to mimic adiabatic quantum tasks at finite time. It has been applied for speeding up adiabaticity in several applications, such as quantum gate Hamiltonians [4–6], heat engines in quantum thermodynamics [7], and quantum information processing [8–10], among others (e.g., Refs. [11–19]). To perform TQD we need to design a *counterdiabatic* Hamiltonian $H_{\rm CD}(t)$, given by $H_{\rm CD}(t) = i\sum_n(|\dot{n}_t\rangle\langle n_t| + \langle\dot{n}_t|n_t\rangle|n_t\rangle\langle n_t|)$, where $\{|n_t\rangle\}$ denotes the set of instantaneous eigenstates of the original adiabatic Hamiltonian $H_0(t)$, and the dot symbol denotes time derivative. The Hamiltonian $H_{\rm CD}(t)$ enables us to cancel any transition between two different eigenstates of $H_0(t)$. It should be added to the original Hamiltonian $H_0(t)$ to yield the *shortcut to adiabaticity* Hamiltonian, which is given by $H_{\rm SA}(t) = H_0(t) + H_{\rm CD}(t)$.

In general, the Hamiltonian $H_{\rm SA}(t)$ allows us to exactly mimic an adiabatic dynamics at arbitrary finite time, so that by starting at a given initial eigenstate $|k_0\rangle$ of $H_0(0)$ the evolved state is given by $|\psi(t)\rangle = e^{i\int_0^t\theta_k^{\rm ad}(\xi)d\xi}|k_t\rangle$, where $\theta^{\rm ad}(t) = -E_n(t) + i\langle n_t|\dot{n}_t\rangle$ is the adiabatic phase [20]. However, there are several applications where we do not need to exactly mimic an adiabatic phase $\theta^{\rm ad}(t)$, as long as the system is kept in an eigenstate of the Hamiltonian $H_0(t)$ [4–19,21–23]. Thus, a generalized approach for TQD has been proposed, where we consider that the phases that accompany the dynamics can be taken as arbitrary [24,25]. Therefore, differently from *traditional* TQD, where the dynamics is driven by $H_{\rm SA}(t) = H_0(t) + H_{\rm CD}(t)$, in *generalized* TQD the dynamics is driven by a generalized shortcut to adiabaticity Hamiltonian $H_{\rm GSA}(t)$ written as [24–26]

$$H_{\rm GSA}(t) = i\sum_n(|\dot{n}_t\rangle\langle n_t| + i\theta_n(t)|n_t\rangle\langle n_t|), \tag{1}$$

where $\theta_n(t)$ are arbitrary real parameters. In this case, the evolved generalized state is written as $|\psi(t)\rangle = e^{i\int_0^t\theta_k(\xi)d\xi}|k_t\rangle$, with arbitrary $\theta_k(t)$. It is worth highlighting that Eq. (1) shows that we can mimic an adiabatic task even when our physical system does not allow for a direct implementation of the adiabatic Hamiltonian. In addition, as it was discussed in Ref. [25], we can also take advantage of these generalized phases $\theta_n(t)$ to simplify the Hamiltonian $H_{\rm GSA}(t)$, possibly even removing in certain situations its dependence on time.

Concerning robustness against decoherence, some experimental and theoretical studies of TQD in different experimental architectures have shown promising features, such as in nitrogen-vacancy setups [21], trapped ions [18], atoms in cavities [9,22], nuclear magnetic resonance (NMR) [23], and optomechanics [19]. These works consider the traditional approach for shortcuts to adiabaticity, where the adiabatic phase

is taken when mimicking the adiabatic dynamics. As theoretically found out in Ref. [25], generalized TQD may provide much better resistance against decoherence depending on the time window designed to run the quantum process.

In this Letter, we report the first experimental implementation aiming at verifying the advantage of generalized TQD with respect to its adiabatic and traditional TQD counterparts. More specifically, we implement the energetically *optimal* version of generalized TQD in a two-level system realizing the Landau–Zener model. Our physical system is composed of a single $^{171}Yb^{+}$ ion confined in a Paul trap, where the system dynamics is driven by the Landau–Zener Hamiltonian. It has previously been shown that the traditional TQD method requires high intensity fields [4–6,27,28]. As we shall see, generalized TQD theory requires much less intense fields while capable of providing better fidelities. In particular, for the dynamics considered here, while traditional TQD requires additional fields, the generalized theory allows us to mimic an adiabatic dynamics without additional fields. Moreover, the dynamics under dephasing shows the superiority of the generalized TQD approach, with higher fidelities with less expenditure of energy resources.

We consider a quantum bit (qubit) undergoing an adiabatic dynamics governed by the Landau–Zener Hamiltonian that reads $H_0(s) = -\Delta\sigma_z - \Omega_R(s)\sigma_x$, with a detuning Δ between the microwave frequency and the atom transition level; $\Omega_R(s)$ is the Rabi frequency, and $s = t/\tau$ is the normalized time. The system is initialized in the ground state $|0\rangle$ of $H_0(0)$ and adiabatically evolves to $|\psi(s)\rangle = e^{-i\tau\int_0^s \theta(\xi)d\xi}|E_+(s)\rangle$, where $|E_+(s)\rangle = \cos[\vartheta(s)/2]|0\rangle + \sin[\vartheta(s)/2]|1\rangle$, with $\vartheta(s) = \arctan[\Omega_R(s)/\Delta]$ a time-dependent dimensionless parameter that satisfies the boundary conditions $\vartheta(0) = 0$ and $\vartheta(1) = \vartheta_0$. Traditional TQD mimics the above dynamics through the Hamiltonian $H_{SA}(s)$, where $H_{CD}(s) = [d_s\vartheta(s)/2\tau]\sigma_y$, with the function $\vartheta(s)$ chosen as $\vartheta(s) = \vartheta_0 s$ for obtaining a time-independent counterdiabatic Hamiltonian (see, e.g., Ref. [25]).

However, in this scenario, we still need to implement a time-dependent contribution due to the adiabatic Hamiltonian $H_0(s)$. On the other hand, if we adopt generalized TQD, we can implement the transitionless dynamics through the simplest time-dependent Hamiltonian given by $H_{OpSA}(s) = H_{CD}(s)$. As in Ref. [25], the energetically optimal Hamiltonian above is obtained by choosing the phases in Eq. (1) through a geometric contribution, such as $\theta_n(t) = i\langle\dot{n}_t|n_t\rangle$, implying here in $\theta_n(t) = 0$. The $H_{OpSA}(s)$ turns out to be implemented by a flat π pulse, whose robustness has been investigated for fast population transfer in Ref. [29].

We now demonstrate the experimental implementation of generalized TQD, with a single $^{171}Yb^{+}$ ion trapped in a six-needle Paul trap, which is shown in Fig. 1(b). We encode a qubit into two hyperfine energy levels of the $^2S_{1/2}$ ground state, denoted by $|0\rangle \equiv {}^2S_{1/2}|F=0, m_F=0\rangle$ and $|1\rangle \equiv {}^2S_{1/2}|F=1, m_F=0\rangle$, as shown in Fig. 1(a). Applying a 6.40 G static magnetic field, the clock transition frequency between $|0\rangle$ and $|1\rangle$ is $\omega_{hf} = 2\pi \times 12.642825$ GHz.

In a configuration of a frequency mixing scheme with an arbitrary waveform generator (AWG), we can coherently drive the hyperfine qubit. The scheme is shown in Fig. 1(c); a $2\pi \times 12.442$ GHz microwave is mixed with the AWG signals around $2\pi \times 200$ MHz to generate the operating waveform. The AWG

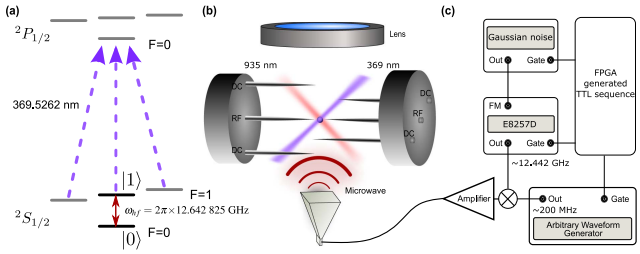

Fig. 1. Experimental setup for implementing the generalized TQD. (a) The energy spectrum of the $^{171}Yb^{+}$ ion, where our two-level system was encoded in the hyperfine energy levels $^2S_{1/2}|F=0, m_F=0\rangle$ and $^2S_{1/2}|F=1, m_F=0\rangle$, and the 369.5 nm laser is used for fluorescence detection. (b) Diagram of the six-needle Paul trap used in our experiment. The microwave horn sends out microwaves to drive the hyperfine qubit and the numerical aperture NA = 0.4 objective lens collects the ion fluorescent photon. (c) Experimental instrument for generating the driving field around $2\pi \times 12.642$ GHz. The Gaussian noise source is used to frequency modulate the driving microwave as a dephasing channel.

waveform is programmed to control ω and Δ for implementing the target Hamiltonian. In addition, to mimic the two-level system interacting with an environment, we introduced a Gaussian noise frequency modulation of the $2\pi \times 12.442$ GHz microwave that can be viewed as a dephasing channel. It is a remarkable fact that the dephasing channel is premium and highly controlled. After Doppler cooling of the trapped ion, we apply a standard optical pumping process to initialize the qubit into the $|0\rangle$ state with 99.9% efficiency. After the qubit operation with microwave sequence, a fluorescence detection method is used to measure the population of the $|1\rangle$ state [30]. The fluorescence of the trapped ion is collected by an optical lens with a numerical aperture of NA = 0.4, passes an optical bandpass filter and a pinhole, and is finally detected by a photomultiplier tube (PMT) with 20% quantum efficiency. Within 300 μs detection time, the target state preparation and measurement fidelity are measured as 99.4% [31].

In our experiment we used both resonant and off-resonant microwave fields to implement adiabatic and TQD dynamics. The adiabatic dynamics was performed by using a nonresonant microwave, where the time-dependent effective Rabi frequency is given by $\Omega_{eff}(s) = [\Omega_R^2(s) + \Delta^2]^{1/2}$. To drive the system by using the traditional TQD, we use an independent microwave to simulate the counterdiabatic term $H_{CD}(s)$. This additional field is a resonant microwave ($\Delta = 0$), whose Rabi frequency can be obtained as $\Omega_{R\text{-}CD}(s) = d_s\vartheta(s)/2\tau$. On the other hand, different from traditional TQD Hamiltonian, the optimal dynamics driven by $H_{GSA}(s)$ could be implemented using a single resonant microwave with Rabi frequency $\Omega_{R\text{-}CD}(s)$, where we have turned off the nonresonant field used for simulate $H_0(s)$.

To quantify the energy resources employed in the quantum evolution, we study the intensity of the fields used to perform the adiabatic dynamics as well as traditional and optimal TQD. The field intensity is associated with the Rabi frequency through the relation $I(s) = \Gamma\Omega_R^2(s)$, where Γ is a constant that depends on the microwave amplifier. Considering the whole evolution time, we can define the average intensity field as $\bar{I}(\tau) = (1/\tau)\int_0^\tau I(t)dt = \int_0^1 I(s)ds$. So, for the adiabatic

dynamics we have $\bar{I}_{\mathrm{Ad}}(\tau) = \Gamma \int_0^1 \Omega_R^2(s)\mathrm{d}s$, for the optimal TQD we get $\bar{I}_{\mathrm{OpSA}}(\tau) = \Gamma \int_0^1 [d_s\vartheta(s)/2\tau]^2\mathrm{d}s$, and for the traditional TQD we find $\bar{I}_{\mathrm{SA}}(\tau) = \bar{I}_{\mathrm{Ad}}(\tau) + \bar{I}_{\mathrm{OpSA}}(\tau)$, since the traditional TQD field is composed by both the adiabatic and the optimal TQD contributions. For convenience, we disregard the constant Γ by taking relative field intensities expressed in unities of the adiabatic intensity $\bar{I}_{\mathrm{Ad}}$. Then, we define $\mathcal{I}_{\mathrm{SA}}(\tau) = \bar{I}_{\mathrm{SA}}(\tau)/\bar{I}_{\mathrm{Ad}}$ and $\mathcal{I}_{\mathrm{OpSA}}(\tau) = \bar{I}_{\mathrm{OpSA}}(\tau)/\bar{I}_{\mathrm{Ad}}$, and adopt the normalization $\mathcal{I}_{\mathrm{Ad}}(\tau) = 1$. These field intensities are plotted in Fig. 2, with a schematic representation of each dynamics indicated in the inset. As we can see from Fig. 2, we can define a value τ_B for the total evolution time for which the intensity fields for implementing optimal TQD becomes less intense than the adiabatic intensity. By computing τ_B we get $\tau_B \approx 0.052$ ms, and we represent this boundary using a vertical line in Fig. 2. Notice that after τ_B, the shortcut to adiabaticity defined by the optimal TQD can be implemented by spending less energy, as measured by the field intensity, than the adiabatic approach.

An alternative approach to compute the energy cost is to estimate the energy scale through the time-average Hamiltonian norm [4–6,25,32]. In this direction, let us consider quantum dynamics driven by a time-dependent Hamiltonian, with energy cost defined as $\Sigma(\tau) = \int_0^\tau \sqrt{\mathrm{Tr}\{H^2(t)\}}\mathrm{d}t$. For the specific case of the Landau–Zener model, this method takes into account not only the external field intensities but also the detuning Δ. Indeed, Δ exerts influence over the energy gap spectrum, which may justify its accounting in some scenarios, such as adiabatic quantum computation. From this definition, we can show that $\Sigma_{\mathrm{SA}}(\tau) \geq \Sigma_{\mathrm{Ad}}(\tau)$, for every τ. Moreover, there is again a boundary value $\tau_{B,\Sigma}$ for which we get $\Sigma_{\mathrm{Op\text{-}SA}}(\tau) < \Sigma_{\mathrm{Ad}}(\tau)$ for $\tau > \tau_{B,\Sigma}$, as originally predicted in Ref. [25]. Here, we obtain $\tau_{B,\Sigma} \approx 0.033$ ms. Thus, we can see that an analysis from the energy scale of the Hamiltonian provides a (qualitatively) equivalent result to the intensity fields analysis. In both cases, it is shown that, by specifically designing a suitable time window, shortcuts to adiabaticity can be implemented in such a way to accelerate physical processes while saving energy resources.

Owing to the long coherence time of the $^{171}Yb^+$ trapped ion hyperfine qubit, the decoherence effects for the timescale adopted in the experimental setup is negligible. Therefore, to simulate the interaction of the Landau–Zener system with an environment, we introduce a Gaussian noise capable of implementing a dephasing channel where the system will be driven by a Lindblad equation given by $\dot{\rho}(t) = -i[H(t), \rho(t)] + \gamma[\sigma_z\rho(t)\sigma_z - \rho(t)]$, where γ is the dephasing rate. To quantify the robustness of the protocols, we use the fidelity $\mathcal{F}(\tau) = \sqrt{\langle\psi(s)|\rho(s)|\psi(s)\rangle}$, which is related to the Bures length [33], with $\rho(s)$ being the solution of the Lindblad equation and $|\psi(s)\rangle = |E_+(s)\rangle$.

We start by disregarding decoherence and implementing each protocol for several choices of $\tau \in [10^{-2}\ \mathrm{ms}, 10\ \mathrm{ms}]$. The results are shown in Fig. 3. Since the maximum total evolution time is $\tau = 10$ ms (i.e., 20 times shorter than the coherence time of the qubit), the dynamics can be considered as approximately unitary. The continuum lines in Fig. 3 show the fidelities $\mathcal{F}(\tau)$ under unitary dynamics for each protocol and the corresponding experimental data points. The black curve shows that the adiabatic behavior is achieved for long total evolution time $\tau \gg \tau_{\mathrm{ad}} \approx 0.021$ ms, with τ_{ad} computed from $\tau_{\mathrm{ad}} = \max_{s\in[0,1]}|\langle E_-(s)|d_sH_0(s)|E_+(s)\rangle/g^2(s)|$, where $g(s) = E_+(s) - E_-(s)$ is the gap between fundamental $|E_-(s)\rangle$ and excited $|E_+(s)\rangle$ energy levels [34]. Notice that, for fast evolutions ($\tau < 0.021$ ms), both optimal TQD and traditional TQD provide a high fidelity protocol, while adiabatic dynamics fails. Naturally, this high performance is accompanied by costly fields used for implementing the TQD protocols, as previously shown in Fig. 2. On the other hand, it is important to highlight that for total evolution time $\tau > \tau_B$, where the optimal TQD field is smaller than both adiabatic and traditional TQD ones, the high performance of optimal TQD is kept. By looking now at the effect of the dephasing channel, we can see that optimal TQD exhibits the highest robustness for every τ, with its advantage increasing as τ increases. For fast

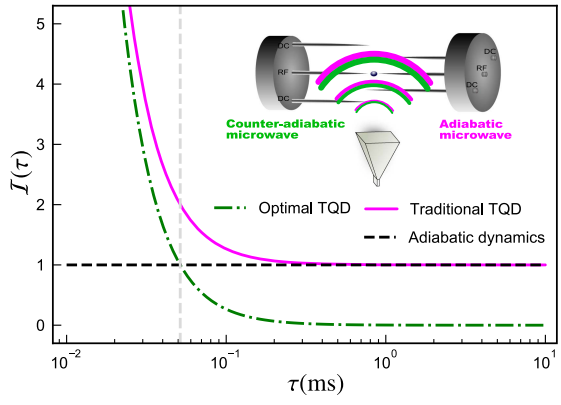

Fig. 2. Calculated relative field intensity $\mathcal{I}(\tau)$ for traditional TQD $\mathcal{I}_{\mathrm{SA}}(\tau)$ (magenta continuum line) and optimal TQD $\mathcal{I}_{\mathrm{OpSA}}(\tau)$ (green dashed–dotted line) as function of the total evolution time τ, where the horizontal black dashed line represents $\mathcal{I}_{\mathrm{Ad}}(\tau)$. The gray vertical line denotes the boundary time $\tau_B \approx 0.052$ ms between the regions $\bar{I}_{\mathrm{OpSA}}(\tau) > \bar{I}_{\mathrm{ad}}(\tau)$ (left-hand side) and $\bar{I}_{\mathrm{OpSA}}(\tau) < \bar{I}_{\mathrm{ad}}(\tau)$ (right-hand side). Inset: schematic representation of the fields used to implement $H_0(s)$, $H_{\mathrm{SA}}(s)$, and $H_{\mathrm{OpSA}}(s)$. We set $\vartheta(s) = \pi s/3$, $\Delta = 2\pi \times 2$ KHz, and $\Omega_R(s) = \Delta\tan(\pi s/3)$ is used in our experiment.

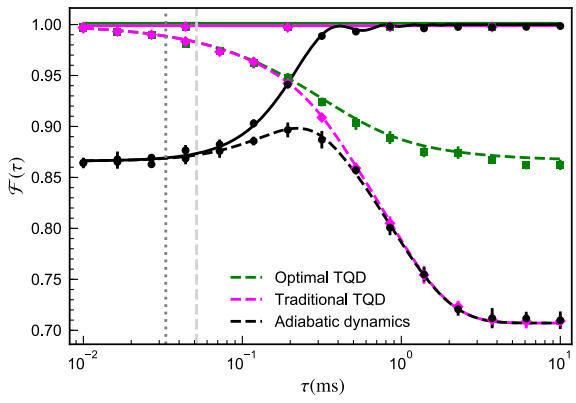

Fig. 3. Fidelity for unitary dynamics (continuum lines) and nonunitary one (dashed lines) under dephasing. The symbols and lines represent experimental data and theoretical results, respectively. We set the Hamiltonian parameter as in Fig. 2, while the decohering rate was kept as $\gamma = 2.5$ KHz for all nonunitary dynamics. The first gray vertical line denotes the boundary time $\tau_B \approx 0.052$ ms as discussed in Fig. 2, while the second vertical line is associated with $\tau_{B,\Sigma} \approx 0.033$ ms.

evolution times, this high performance is again associated with costly fields in comparison to the adiabatic fields. However, for large evolution times, while the traditional TQD fidelity converges to adiabatic fidelity, the fidelity behavior of optimal TQD is much better than both adiabatic dynamics and traditional TQD, with less energy spent in the process. This is a remarkable result, since we can achieve both better fidelities with fewer energy fields involved, where we get $\mathcal{F}_{\mathrm{OpSA}} > \mathcal{F}_{\mathrm{Ad}}$ even when $\bar{I}_{\mathrm{OpSA}} \ll \bar{I}_{\mathrm{Ad}}$.

In this Letter we have experimentally investigated the performance of shortcuts to adiabaticity by exploiting the gauge freedom as we fix the phase accompanying the evolution dynamics. In particular, we have focused on the optimal TQD, comparing it to its associated adiabatic dynamics and traditional TQD counterparts. Our main results follow. First, the optimal version of generalized TQD has been shown to be a useful protocol for obtaining the optimal shortcut to adiabaticity. While adiabatic and traditional TQD require time-dependent quantum control, optimal TQD can be experimentally realized by using time-independent fields. In addition, the necessity of auxiliary fields in traditional TQD is not a requirement for implementing TQD via its optimal version. Second, optimal TQD is an energetically optimal protocol of shortcut to adiabaticity. By considering the average intensity fields as a measure of energy cost for implementing the protocols discussed here, we were able to show that the optimal version of generalized TQD may be energetically less demanding. This result is kept also for alternatives definitions of energy cost, e.g., taking into account the detuning contribution. Third, by simulating an environment-system coupling associated with the dephasing channel, we have shown that optimal TQD can be more robust than the adiabatic dynamics and the traditional TQD while at the same time spending less energy for a finite time range. In addition, we were able to mimic the adiabatic behavior through time-independent Hamiltonian, showing that the optimal theory works. Once the Landau–Zener Hamiltonian can be implemented in other physical systems, e.g., nuclear magnetic resonance [35] and two-level systems driven by a chirped field [1], it is reasonable to think that the results obtained here can be also realized in other experimental architectures. Moreover, inverse engineering protocols are an interesting candidate to implement fast and robust elementary quantum gates for quantum computing [4–6,36]. Thus, an experimental investigation of these protocols can be a promising direction as future research, as can the robustness of optimal TQD compared to other classes of errors (as it has been done for traditional TQD in Ref. [37]).

Funding. National Key Research and Development Program of China (2017YFA0304100); National Natural Science Foundation of China (NSFC) (11304305, 11374288, 11404319, 11474268, 11734015, 11774335, 61327901, 61490711); Anhui Initiative in Quantum Information Technologies (AHY070000); Key Research Program of Frontier Sciences, Chinese Academy of Sciences (CAS) (QYZDY-SSWSLH003); National Program for Support of Top-notch Young Professionals (BB2470000005); Fundamental Research Funds for the Central Universities (WK2470000026); CNPq-Brazil (303070/2016-1); Fundação Carlos Chagas Filho de Amparo à Pesquisa do Estado do Rio de Janeiro (203036/2016).

Acknowledgment. A. C. S. is supported by CNPq-Brazil. M. S. S. is supported by CNPq-Brazil, FAPERJ, and the Brazilian National Institute for Science and Technology of Quantum Information (INCT-IQ).

[†]These authors contributed equally for this work.

REFERENCES

1. M. Demirplak and S. A. Rice, J. Phys. Chem. A **107**, 9937 (2003).
2. M. Demirplak and S. A. Rice, J. Phys. Chem. B **109**, 6838 (2005).
3. M. Berry, J. Phys. A **42**, 365303 (2009).
4. A. C. Santos and M. S. Sarandy, Sci. Rep. **5**, 15775 (2015).
5. A. C. Santos, R. D. Silva, and M. S. Sarandy, Phys. Rev. A **93**, 012311 (2016).
6. I. B. Coulamy, A. C. Santos, I. Hen, and M. S. Sarandy, Front. ICT **3**, 19 (2016).
7. M. Beau, J. Jaramillo, and A. del Campo, Entropy **18**, 168 (2016).
8. M. Herrera, M. S. Sarandy, E. I. Duzzioni, and R. M. Serra, Phys. Rev. A **89**, 022323 (2014).
9. Z. Chen, Y. Chen, Y. Xia, J. Song, and B. Huang, Sci. Rep. **6**, 22202 (2016).
10. X. Chen, I. Lizuain, A. Ruschhaupt, D. Guéry-Odelin, and J. G. Muga, Phys. Rev. Lett. **105**, 123003 (2010).
11. D. Stefanatos, Phys. Rev. A **90**, 023811 (2014).
12. M. Lu, Y. Xia, L.-T. Shen, J. Song, and N. B. An, Phys. Rev. A **89**, 012326 (2014).
13. S. Deffner, New J. Phys. **18**, 012001 (2016).
14. Y.-H. Chen, Y. Xia, Q.-Q. Chen, and J. Song, Phys. Rev. A **89**, 033856 (2014).
15. X.-K. Song, H. Zhang, Q. Ai, J. Qiu, and F.-G. Deng, New J. Phys. **18**, 023001 (2016).
16. A. del Campo, Phys. Rev. Lett. **111**, 100502 (2013).
17. H. Saberi, T. Opatrný, K. Mølmer, and A. del Campo, Phys. Rev. A **90**, 060301 (2014).
18. S. An, D. Lv, A. Del Campo, and K. Kim, Nat. Commun. **7**, 12999 (2016).
19. H. Zhang, X.-K. Song, Q. Ai, M. Zhang, and F.-G. Deng, "Transitionless intra-cavity quantum state transfer in optomechanical systems," arXiv: 1610.09938 (2016).
20. M. V. Berry, Proc. R. Soc. A **392**, 45 (1984).
21. Z.-T. Liang, X. Yue, Q. Lv, Y.-X. Du, W. Huang, H. Yan, and S.-L. Zhu, Phys. Rev. A **93**, 040305 (2016).
22. S. L. Wu, X. L. Huang, H. Li, and X. X. Yi, Phys. Rev. A **96**, 042104 (2017).
23. J. Vandermause and C. Ramanathan, Phys. Rev. A **93**, 052329 (2016).
24. E. Torrontegui, S. Ibáñez, S. Martínez-Garaot, M. Modugno, A. Del Campo, D. Guéry-Odelin, A. Ruschhaupt, X. Chen, and J. G. Muga, Adv. At. Mol. Opt. Phys. **62**, 117 (2013).
25. A. C. Santos and M. S. Sarandy, J. Phys. A **51**, 025301 (2018).
26. X. Chen, E. Torrontegui, and J. G. Muga, Phys. Rev. A **83**, 062116 (2011).
27. S. Campbell and S. Deffner, Phys. Rev. Lett. **118**, 100601 (2017).
28. O. Abah and E. Lutz, Europhys. Lett. **118**, 40005 (2017).
29. X.-J. Lu, X. Chen, A. Ruschhaupt, D. Alonso, S. Guérin, and J. G. Muga, Phys. Rev. A **88**, 033406 (2013).
30. S. Olmschenk, K. C. Younge, D. L. Moehring, D. N. Matsukevich, P. Maunz, and C. Monroe, Phys. Rev. A **76**, 052314 (2007).
31. R. Blume-Kohout, J. K. Gamble, E. Nielsen, K. Rudinger, J. Mizrahi, K. Fortier, and P. Maunz, Nat. Commun. **8**, 14485 (2017).
32. M. Kieferová and N. Wiebe, New J. Phys. **16**, 123034 (2014).
33. D. Bures, Trans. Am. Math. Soc. **135**, 199 (1969).
34. M. S. Sarandy, L.-A. Wu, and D. A. Lidar, Quantum Inf. Process. **3**, 331 (2004).
35. M. A. Nielsen and I. L. Chuang, *Quantum Computation and Quantum Information*, 10th ed. (Cambridge University, 2011).
36. A. C. Santos, J. Phys. B **51**, 015501 (2018).
37. A. Ruschhaupt, X. Chen, D. Alonso, and J. Muga, New J. Phys. **14**, 093040 (2012).

222.195.68.69 {ts '2019-10-13 21:59:24'}